Communication

Glycosidic Linkage Rotations Determine Amylose Stretching Mechanism

Michelle Kuttel, and Kevin J. Naidoo

J. Am. Chem. Soc., **2005**, 127 (1), 12-13• DOI: 10.1021/ja047138s • Publication Date (Web): 09 December 2004

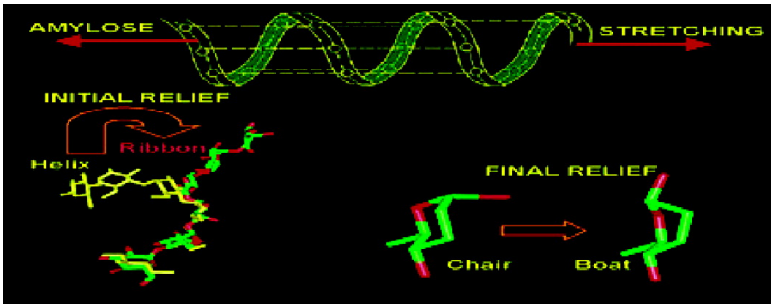

More About This Article

Additional resources and features associated with this article are available within the HTML version:

- Supporting Information
- Links to the 3 articles that cite this article, as of the time of this article download
- Access to high resolution figures
- Links to articles and content related to this article
- Copyright permission to reproduce figures and/or text from this article

View the Full Text HTML

J|A|C|S
COMMUNICATIONS

Published on Web 12/09/2004

Glycosidic Linkage Rotations Determine Amylose Stretching Mechanism

Michelle Kuttel and Kevin J. Naidoo*

Centre for High Performance Computing, Western Cape, South Africa, and Department of Chemistry, University of Cape Town, Rondebosch 7701, South Africa

Received May 16, 2004; E-mail: knaidoo@science.uct.ac.za

Molecular elasticity in saccharides is often thought to be a function of both rotational motion about the glycosidic bonds and the flexibility of the sugar rings themselves. Stretching experiments on single molecules using atomic force microscopy (AFM) produced distinctive "fingerprint" force−extension curves for various glucose polysaccharides differing only in the locations of their glycosidic linkages.[1−5] Moreover, only the α-linked molecules have characteristic plateaus in their force−extension curves,[2,4] whereas inelastic β-linked cellulose does not.[3] This yielding behavior has been attributed to transitions of the α-linked glucose rings from the $^4C_1$ chair to a twist-boat conformation.[3−7] Here we show through stretching simulations in combination with free energy calculations the unfolding pattern for amylose and that the primary mechanism for relieving tensile strain in α-linked polysaccharides such as amylose [α-D-Glc-(1→4)α-D-Glc]$_n$ involves complex rotations of the glycosidic linkages, while chair-to-boat conversions of the pyranose rings play a smaller role.

Stretching simulations and free energy calculations were performed using CHARMM (version 27b1)[8] incorporating our modifications to the USERE routine. An 18-unit amylose fragment was stretched by applying equal but opposite forces to the reducing and nonreducing ends of the chain. The applied force was incrementally increased during the simulation, followed by 1ns of equilibration and 15−20 ns of data collection. This produced a force−extension profile for amylose (Figure 1a) which exhibits the distinctive transitions seen in AFM stretching experiments.[1,5] The key to this favorable comparison with the experimental curve (Figure 1a) is the thorough sampling of conformational space during the stretching simulation. Both simulated and experimental curves display four distinct stages labeled I−IV.

Each region corresponds to a different conformational transition. From an initial helical conformation, the oligomer strand relieves tensile strain by rotating the glycosidic linkage torsion angles resulting in a more extended helix (stage I). To establish the entire range of motion for the glycosidic linkages in an amylose strand, we calculated the β-maltose Ramachandran free energy surface as a function of the ϕ,ψ dihedrals (Figure 1b). The ϕ and ψ dihedral angles for the α(1→4)-linkage are defined as ϕ = H1−C1−O1−C4′, ψ = C1−O1−C4′−H4′. This surface corresponds with adiabatic maltose maps[9] and is characterized by two principal minimum energy valleys, designated by the conformations *syn* ($\psi = 0°$) and *anti* ($\psi = 180°$). Conformational changes in stage I of the amylose stretching curve correspond with a ϕ,ψ rotation toward a more negative region of the global minimum energy well.

During the gradual transition from stages I to II the amylose strand switches from a helical conformation to a flatter "ribbon" conformation. The underlying molecular mechanism is due to a forced rotation of most of the glycosidic ψ dihedral angles from *syn* to *anti* conformations so that any helical character of the strand is disrupted. The glycosidic linkages are subjected to further strain in stage II, resulting in a slight lengthening of the stiff ribbon conformation.

A very steep slope signifies the rapid onset of stage III in the amylose stretching profile. Despite 2 of the 18 pyranose rings converting from a chair to a boat conformation, these transitions are not the dominating process for relieving strain at this stage of stretching. In fact the rapid increase in length is due primarily to the ψ dihedrals reverting from *anti* to *syn*, thereby producing a maximally extended helical conformation.

An end-to-end distance−free energy profile for a maltohexaose oligosaccharide was calculated in a vacuum by applying an umbrella potential to ends of the molecule, similar to that undertaken for peptide structures[10] (Figure 1c). This provides an energetic rationale for the role that the torsions play in the complex helix−ribbon−helix conformational transition in amylose stretching. The end-to-end global minimum occurs at $r = 0.2$ (where r is normalized relative to the maximum extension) representing near macrocyclic conformations that are stable in a vacuum. The second minimum, ranging from $r = 0.4$ to $r = 0.6$, is of greater interest here and encompasses extended conformations that can be broadly classified into helices (all ψ's are *syn*) and ribbonlike shapes (some ψ's are *anti*).

Stretching the chain to lengths of $r > 0.8$ provides sufficient energy to overcome the *syn*-to-*anti* energy barrier (10 kcal/mol of energy−transition marked I/II in Figure 1b). Transitions typically occurred at the central point of the chain (ψ_3), which is the focus of the stretching force. The two ψ_3-dependent end-to-end distance−energy surfaces represent the helical (ψ_3 = *syn*) and ribbon (ψ_3 = *anti*) conformations, respectively, and explain the relative contribution of these conformations to the total free energy (Figure 1c). At short extensions the helical curve is lowest in energy and similar to the overall curve for all conformations. However, in the $r = 0.66−0.86$ region the ribbon contour is energetically lower than the helix contour, indicating that significant numbers of ribbon conformers are included in the total population of stretched strands. This corresponds to stage II of the AFM curve. Interestingly, the ribbon and helix curves cross again at $r = 0.87$, resulting in helical conformations being more favored at very long extensions (stage III). Thus, moderate stretching favors ribbon conformations, while more severe stretching favors helices.

By the end of stage III of the stretching profile, the extension of the amylose molecule approaches its contour length, and further rotations of the ϕ,ψ glycosidic dihedral angles can no longer lengthen the chain. It is here (stage IV) that the majority of the chair-to-boat transitions of the pyranose rings occurs. These conversions occur at higher forces and at a different stage of the force−extension curve than previously proposed (stage IV, not stage III) and are not responsible for the characteristic "shoulder" in the amylose stretching curve. The amylose stretching mechanism (Figure 2) is dominated by the rotational freedom of the glycosidic linkages with chair-to-boat conversions possibly playing a minor

 10.1021/ja047138s CCC: $30.25

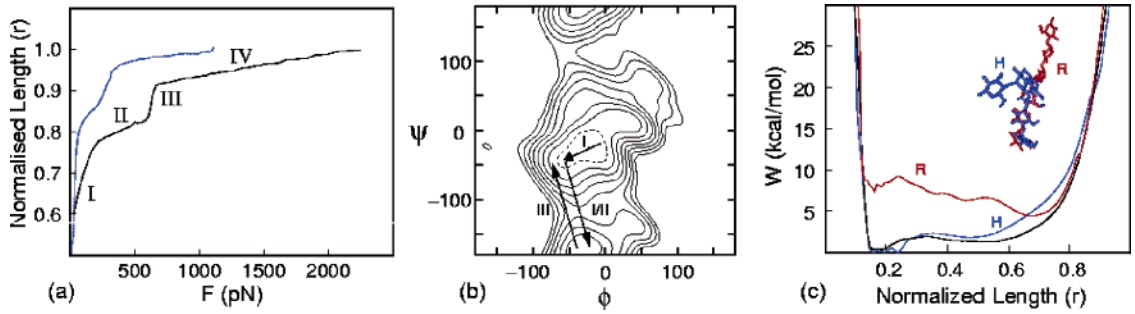

Figure 1. Amylose stretching dynamics. (a) Normalized simulated force−extension curve of an 18-unit amylose oligomer (black line) compared with the AFM amylose experiment[1] (blue line). (b) Maltose ϕ,ψ free energy surface in a vacuum. Contoured at 2 kcal/mol intervals (lowest-energy contour dashed). Arrows indicate glycosidic linkage transitions occurring in the first three stages of the amylose force−extension curve. (c) Maltohexaose normalized end-to-end distance−free energy curves in a vacuum: helical (H, blue line), ribbon (R, red line), and all conformations (black line).

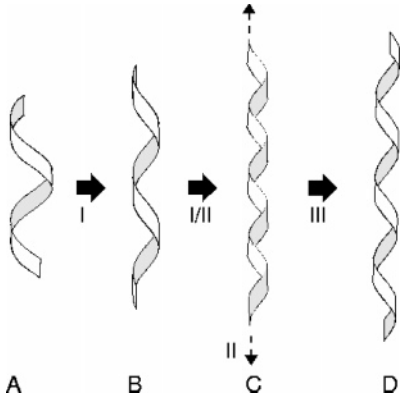

Figure 2. A schematic diagram of the unfolding mechanism for stages I to III of the amylose force−extension curve. Transitions are made from a relaxed helix (A), to a more extended helix (B), to a ribbon (ψ are *anti*) conformations (C), finally returning to a very extended helix (D).

role. The removal of the chain elasticity of amylose upon ring cleavage with periodate[4] supports this proposal as steric hindrances to glycosidic linkage rotation will be reduced, resulting in an altered force extension relationship. Ab initio calculations of chair-to-boat conversions in pyranose monomers show transition-energy barriers of approximately 14 kcal/mol[7] with the microsecond range being the *shortest* time required for barrier crossover at 275 pN pulling strength. In contrast to this is the complete reversibility of stages I to III of the AFM experiments, suggesting a mechanism involving relatively low transition-energy barriers.[1]

Our recent ab initio and nanosecond molecular dynamics studies of solvated disaccharides[11] revealed a competition between the intermolecular water−maltose and intramolecular hydrogen bonds of comparable strengths in maltose which leads to water promoting rotation about the glycosidic bond. More pertinent here is the shift of the global minimum to more negative values in the full maltose solution ϕ,ψ free energy surface, compared with the vacuum surface (Figure 1b).[12] The *syn* to *anti* rotational barrier is therefore lowered. We therefore expect that aqueous solvent in the AFM experiments will decrease the force required for stages I (helix lengthening) and II (ϕ rotations), but not significantly so for stages III and IV.

Acknowledgment. K.J.N. thanks the USDA for partial support from USDA-ARS Grant 58-4012-5-F120. M.K. thanks the University of Cape Town for doctoral support.

Supporting Information Available: Methods and conditions, for stretching and free energy simulations. This material is available free of charge via the Internet at http://pubs.acs.org.

References

(1) Marszalek, P. E.; Pang, Y.-P.; Li, H.; Yazal, J. E.; Oberhauser, A. F.; Fernandez, J. M. *Proc. Natl. Acad. Sci. U.S.A.* **1999**, *96*, 7894−7898.
(2) Rief, M.; Oesterhelt, M.; Heymann, B.; Gaub, H. E. *Science* **1997**, *275*, 1295−1297.
(3) Li, H.; Rief, M.; Oesterhelt, F.; Gaub, H. E.; Zhang, X.; Shen, J. *Chem. Phys. Lett.* **1999**, *305*, 197−201.
(4) Marszalek, P. E.; Oberhauser, A. F.; Pang, Y.-P.; Fernandez, J. M. *Nature* **1998**, *396*, 661−664.
(5) Marszalek, P. E.; Li, H.; Oberhauser, A. F.; Fernandez, J. M. *Proc. Natl. Acad. Sci. U.S.A.* **2002**, *99*, 4278−4283.
(6) (a) Heymann, B.; Grubmuller, H. *Chem. Phys. Lett.* **1999**, *305*, 202−208. (b) Lu, Z.; Nowak, W.; Lee, G.; Marszalek, P. E.; Yang, W. *J. Am. Chem. Soc.* **2004**, *126*, 9033−9041.
(7) O'Donoghue, P.; Luthey-Schulten, Z. A. *J. Phys. Chem. B* **2000**, *104*, 10398−10405.
(8) Brooks, B. R.; Bruccoleri, R. E.; Olafson, B. D.; States, D. J.; Swaminathan, S.; Karplus, M. *J. Comput. Chem.* **1983**, *4*, 187−217.
(9) (a) Ha, S. N.; Madsen, L. J.; Brady, J. W. *Biopolymers* **1988**, *27*, 1927−1952. (b) Brant, D. A. *Pure Appl. Chem.* **1997**, *69*, 1885−1892. (c) Best, R. E.; Jackson, G. E.; Naidoo, K. J. *J. Phys. Chem. B* **2001**, *105*, 4742−4751. (d) Naidoo, K. J.; Kuttel, M. M. *J. Comput. Chem.* **2001**, *22*, 445−456.
(10) (a) Brooks, C. L., III; Case, D. A. *Chem. Rev.* **1993**, *93*, 2487−2502. (b) Kadkhodaei, M.; Wu, H.; Brant, D. A. *Biopolymers* **1991**, *31*, 1581−1592.
(11) (a) Chen, Y.-J.; Naidoo, K. J. *J. Phys. Chem. B* **2003**, *107*, 9558−9566. (b) Naidoo, K. J.; Chen, Y.-J. *Mol. Phys.* **2003**, *101*, 2687−2694.
(12) Kuttel, M. M.; Naidoo, K. J. *J. Phys. Chem. B* Manuscript submitted.

JA047138S